

C₆₀ in Water: Nanocrystal Formation and Microbial Response

J. D. FORTNER,^{†,‡} D. Y. LYON,^{†,‡}
 C. M. SAYES,^{‡,§} A. M. BOYD,^{‡,§}
 J. C. FALKNER,[§] E. M. HOTZE,^{†,‡}
 L. B. ALEMANY,[§] Y. J. TAO,^{||,⊥} W. GUO,[§]
 K. D. AUSMAN,[‡] V. L. COLVIN,^{‡,§} AND
 J. B. HUGHES^{*,†,⊥}

Department of Civil and Environmental Engineering, Rice University, Houston, Texas 77005, Department of Chemistry, Rice University, Houston, Texas 77005, Department of Biochemistry and Cell Biology, Rice University, Houston, Texas 77005, Center for Biological and Environmental Nanotechnology, Rice University, Houston, Texas 77005, and School of Civil and Environmental Engineering, Georgia Institute of Technology, Atlanta, Georgia 30332

Upon contact with water, under a variety of conditions, C₆₀ spontaneously forms a stable aggregate with nanoscale dimensions ($d = 25\text{--}500$ nm), termed here "nano-C₆₀". The color, hydrophobicity, and reactivity of individual C₆₀ are substantially altered in this aggregate form. Herein, we provide conclusive lines of evidence demonstrating that in solution these aggregates are crystalline in order and remain as underivatized C₆₀ throughout the formation/stabilization process that can later be chemically reversed. Particle size can be affected by formation parameters such as rates and the pH of the water addition. Once formed, nano-C₆₀ remains stable in solution at or below ionic strengths of 0.05 M for months. In addition to demonstrating aggregate formation and stability over a wide range of conditions, results suggest that prokaryotic exposure to nano-C₆₀ at relatively low concentrations is inhibitory, indicated by lack of growth (≥ 0.4 ppm) and decreased aerobic respiration rates (4 ppm). This work demonstrates the fact that the environmental fate, distribution, and biological risk associated with this important class of engineered nanomaterials will require a model that addresses not only the properties of bulk C₆₀ but also that of the aggregate form generated in aqueous media.

Introduction

Over the past 20 years, carbon fullerenes have been extensively studied; their unique properties make them ideal candidates for widespread applications in areas as diverse as drug delivery and energy conversion (1–7). As industrial scale production of fullerenes approaches reality (Frontier Carbon Corporation estimates production of ~10 tons of fullerene per year, as C₆₀, by 2007), it is not surprising that

little is known about the potential impact of fullerenes on natural systems (8). For example, current OSHA guidelines for handling and disposal of C₆₀ follow the MSDS of simple carbon black. Furthermore, recent studies by Sayes et al. (9) and Oberdörster (10) have demonstrated that fullerenes, as C₆₀ in an aggregate form, can elicit a biological response at relatively low concentrations (<1 ppm). Such findings take on additional significance as fullerenes have been found in particulate matter emitted from coal-fired power plants (11). The purpose of this research is to begin assessing fullerene behavior in the natural environment. More specifically, we begin to assess C₆₀ as it comes into contact with water, observing the form(s) these materials may take and consider the ecological risk associated with exposure.

Carbon-60 (C₆₀), the prototypical carbon-based nanoparticle, is arguably the most well-studied engineered nanomaterial to date. In particular, the low solubility of C₆₀ in polar solvents such as water ($< 10^{-9}$ mg/L) is well-accepted (12–14). However, as demonstrated by this study and others, direct solubility is not the most relevant measure of the availability of fullerenes in water-based systems (15–19). Upon contact with water through several different exposure methods, C₆₀ forms a water-stable, colloidal aggregate referred to here as "nano-C₆₀" to reflect that the aggregates are composed of C₆₀ with reported diameters from ~5 to 500 nm (18–20). These aggregates allow for concentrations up to 100 mg/L, which is ~11 orders of magnitude more than the estimated molecular solubility (12–14). Though this material has been the subject of some study over the past decade, questions concerning the formation, composition, and stability of nano-C₆₀ remain unresolved (16, 18–21).

The early interest in aggregate forms of fullerenes, particularly nano-C₆₀, was motivated by their applications in technologies, particularly those that require fullerenes in water (16–18). Nano-C₆₀ has shown little promise in this regard, as typical concentrations (<100 ppm) are far below the 10 000–100 000 ppm levels that are achievable when the carbon cage is intentionally altered to include polar functionalities (22–27). Still, such aggregate generation through unintentional exposure of fullerenes to water is possible, and the amounts generated may be significant for ecological effects (≤ 100 ppm). Other lipophilic organic molecules, which might be analogous to C₆₀, have significant ecological impact in aqueous systems at concentrations of 1–10 ppm (28).

Specifically, research presented herein addresses outstanding questions and expands upon what is currently known about the composition, formation, stability, and potential biological effects of nano-C₆₀. We provide original information concerning the physical and chemical structure of nano-C₆₀ directly in water using ¹³C NMR, cryogenic transmission electron microscopy (cryo-TEM), and electron diffraction. These analyses demonstrate that nano-C₆₀ is an ordered crystal structure comprised of underivatized C₆₀. We found that the size and stability of these materials are affected by the conditions of formation, which include the rate of water addition and solution pH. Once the nano-C₆₀ aggregates are formed, the stability is variable, depending on the ionic strength of the solution. A bacterial (Gram-positive and Gram-negative) response to these particles was studied and compared with similar concentrations of a soluble derivative as C₆₀(OH)_{22–24} and a negative control lacking fullerenes. Results suggest that exposure to nano-C₆₀ at relatively low concentrations is inhibitory, indicated by lack of growth and decreased aerobic respiration rates. This is, to our knowledge, the first examination of the response of bacteria to nano-C₆₀.

* Corresponding author phone: (404)894-2201; fax: (404)894-2278; e-mail: joseph.hughes@ce.gatech.edu.

[†] Department of Civil and Environmental Engineering, Rice University.

[‡] Center for Biological and Environmental Nanotechnology, Rice University.

[§] Department of Chemistry, Rice University.

^{||} Department of Biochemistry and Cell Biology, Rice University.

[⊥] School of Civil and Environmental Engineering, Georgia Institute of Technology.

Materials and Methods

Chemicals. C₆₀ (99.9% purified through sublimation), ¹³C-enriched C₆₀ (25% of carbon labeled, 99.5% pure), and C₆₀(OH)_{22–24} (prepared through a brominated intermediate; 29) were purchased from the Materials Electronics Research Corporation (Tucson, AZ). All water used was ultra-purified to > 18 Ω (Millipore Synergy system).

Nano-C₆₀ Preparation. As large volumes of solutions were used throughout the study, a reproducible and relatively simple preparation of nano-C₆₀ was modified from Deguchi et al. (19) as follows. Approximately 100 mg of C₆₀ was added to 4 L of previously unopened tetrahydrofuran (THF) (spectroanalyzed, >99.99%, Fisher Scientific) and sparged with N₂ to remove oxygen. Upon resealing the THF–C₆₀ mixture, the solution was left for 24 h stirring at ambient temperature, allowing it to become saturated with soluble C₆₀ (9 mg/L solubility in THF) (19). Upon saturation, the solution was then vacuum filtered through a 0.22 μm nylon membrane (Osmotics Corp.), resulting in a transparent solution with a pink hue, which was sparged with N₂ and stored in the dark for later use. The C₆₀-saturated THF solution was added (250 mL) to a 2 L wide mouth Erlenmeyer flask and stirred rapidly. To this solution, ultrapure water (250 mL) at pH 5 (the pH of the water taken directly from the Milli-Q system) was added at 500 mL/min to the stirring THF. Mixing experiments were done similarly except by varying the rate of water addition (1000, 500, 250, 125, 63, 31, and 10 mL/min). The role pH in the formation processes was evaluated by carefully adjusting the pH of the water added (500 mL/min) with dilute NaOH or HCl. As the water was added, the mixed solution changed from a pink to a transparent yellow solution. Using a rotary evaporator (Buchi Rotovap system), the mixed solution was gently heated (75–80 °C), collecting the more volatile THF. To ensure a consistent level of THF removal from solution, a stepwise evaporating procedure was used as follows. Starting with 1 L total volume (1:1, water:THF), approximately 550 mL was evaporated and collected. The remaining yellow solution was diluted with 100 mL of water. The solution was then evaporated again to 450 mL and then diluted with 100 mL of water. Finally, the solution was evaporated again to the final volume of 500 mL. This solution was transferred and left to cool overnight at room temperature. The solution was then vacuum filtered (0.22 μm cellulose acetate, Corning Inc.) into a 500 mL sterile container and stored in the dark. To concentrate the suspensions, a protein concentrating centrifugal cartridge was used with a 30 000 MWCO (Amicon Ultra 15, Millipore). A total of 10 mL of suspension was added to each cartridge and centrifuged for 15 min at 5000 rpm. After each time, the approximately 500 μL of concentrated solution remained in the receptacle, which was diluted with 10 mL of the original suspension and centrifuged as mentioned until the desired concentration was reached.

Particle Stability. Stability of these suspensions was evaluated at different ionic strengths over time. A nano-C₆₀ suspension prepared with water at pH 5 added at 500 mL/min was subdivided and prepared at different ionic strength (*I*) by the addition of NaCl. A range of ionic strengths (0.7, 0.1, 0.05, 0.01, 0.001 *I*) from approximately seawater (0.7 *I*) to groundwater (0.01 *I*) and below was investigated. Particle stability and size was evaluated over time with dynamic light scattering (ZetaPALS, Brookhaven Instruments Corporation, Holtsville, NY).

Concentration Determination. The concentrations of C₆₀ in THF, toluene, and hexane were determined from the absorption spectrum. The concentration of C₆₀ as a nanoscale suspension in water was determined through a two-step destabilization–extraction process as follows: One volume of water with suspended nano-C₆₀ particles was destabilized

with 2/5 volume 0.1 M Mg(ClO₄)₂ and extracted with one volume toluene (as a separate phase), in which molecular C₆₀ is soluble at 2.8 mg/mL (12). When compared to other oxidizing agents tested, Mg(ClO₄)₂ provided consistent destabilization of nano-C₆₀ over a range of pH values (5–9), allowing for a high extraction efficiencies (94–101%). If no destabilizing agent was used, extraction efficiencies were low (≤10%). The two-phase system was sealed and vigorously mixed for 30 min. After extraction into the organic phase was complete, the water portion of the system was frozen in a dry ice bath allowing for removal of the toluene portion containing the dissolved C₆₀. HPLC analysis was performed on toluene solutions. C₆₀ eluted at 5.6 min (4.6 × 250 mm Cosmosil PYE column, 1 mL/min toluene mobile phase) with characteristic C₆₀ absorption peaks at 336, 407, 540, and 595 nm observed. The 5.6 min C₆₀ peak from the extraction consistently represented ≥98% of the total chromatograph peak integration (30). This procedure was verified through the use of a gravimetric procedure, using a microbalance, evaporating 2 mL of a 100 mg/L concentrated suspension determining the weight of suspended nano-C₆₀ in water.

Characterization. All reported UV/Vis absorption spectra were taken within a range of 190–800 nm (Varian Cary 5000 UV–Vis–NIR, at 0.5 nm intervals) at room temperature and corrected for the appropriate solvent background. A 100 mg/L nano-C₆₀ suspension prepared with ¹³C-enriched C₆₀ (25%) in D₂O was analyzed using a 500 MHz NMR (Bruker Avance, Germany) with a broadband observe probe. The experiment used a 30° ¹³C pulse, 2.36-s FID with proton decoupling, and 5-s relaxation delay with proton decoupling taking 7680 scans over 15.7 h. Proton decoupling was used to narrow and to detect any ¹³C signals from proton-containing species that might be present. The FID was processed with 5 Hz of line broadening to further increase signal-to-noise ratio. The chemical shift scale of this sample, dissolved in D₂O, is relative to the trimethylsilyl group defined as 0 ppm in (CH₃)₃Si–CD₂–CD₂–COONa dissolved in D₂O. Average ζ potential of the particles in solutions was measured using a ZetaPALS (Brookhaven Instruments Corporation) at room temperature. Particle size and shape were analyzed by two methods: dynamic light scattering (DLS) using a ZetaPALS and transmission electron microscopy, the latter of which provided dimensional information. Two types of transmission electron microscope images were taken. First, traditional dried images were prepared by evaporating two drops of concentrated suspension on a 400 mesh carbon-coated copper grid and imaged with a JEOL FasTEM 2010 transmission electron microscope at 100 kV. The microscope camera length was calibrated using an aluminum standard. In addition, flash-frozen suspensions were imaged with a transmission electron microscope outfitted with a cryogenic sample holder (JEOL FasTEM 2010). To aid in these image analyses, Image Pro software was used.

Microbial Assays. The ability of Gram-negative *Escherichia coli* DH5α and Gram-positive *Bacillus subtilis* CB315 (JH642 derivative; a facultative anaerobe capable of reducing nitrate under anaerobic conditions (31)) to grow in the presence of nano-C₆₀ was studied at pH 7 using both a rich (Luria broth; LB) and a minimal media (minimal Davis media with 10% of the recommended potassium phosphate; MD) with glucose as the carbon and electron source (1 g/L) (32). For all anaerobic experiments, KNO₃ was used as an electron acceptor. Cultures were incubated at a constant temperature of 37 °C with and without the presence of light while shaking (aerobic growth) or static in an anaerobic chamber (anaerobic growth) (33). In triplicate, batch studies were inoculated with fresh overnight cultures of bacteria to an OD at 600 nm of 0.002. Growth was monitored similarly at 600 nm in 24-h increments and verified with plate counts (data not shown). Different concentrations of nano-C₆₀ (0.04, 0.4 mg/L 4 mg/L

L) along with $C_{60}(OH)_{22-24}$ (5 mg/L) were compared to a negative control that lacked any fullerene. Results were reported simply as yes (+) growth occurred or no (-) growth did not occur (Table 1). Aerobic respiration of both cultures suspended in MD media (as described above) was monitored via CO_2 production rates over time with a 10-chamber respirometer (Columbus Instruments, Columbus, OH) at room temperature (20–22 °C) (34). At mid-exponential phase, the bottles were amended with a varying concentration of nano- C_{60} , $C_{60}(OH)_{22-24}$, or no fullerene as a negative control. Results are presented as accumulative CO_2 production over time.

Results

When exposed to water, C_{60} can form “hydrophilic” colloids that are stable in water (9, 15–19). This form of C_{60} does not extract appreciably back into a nonpolar solvent, such as toluene, indicating that the process leading up to colloid formation fundamentally alters the properties of the fullerene. (Figure 1A). Ultraviolet visible (UV/Vis) analysis of these yellow suspensions finds characteristic peaks of solvated C_{60}

in solution between 330 and 350 nm; however, an additional broad 400–500 nm absorption is also apparent (Figure 1B) (19, 21). This feature is characteristic of solid-state, crystalline C_{60} and arises from close electronic interactions among adjacent C_{60} molecules. Depending on the form and density of C_{60} crystals, this absorbance has an initial appearance between 450 and 600 nm (35, 36).

Molecular analysis of these crystal suspensions using high-pressure liquid chromatography (HPLC), absorption spectroscopy, and NMR indicates that nano- C_{60} is comprised predominantly of underivatized C_{60} . HPLC analysis was completed after nano- C_{60} was briefly treated with a mild oxidizing agent (e.g., 0.05 M $Mg(ClO_4)_2$); destabilizing the aggregates allowing for complete extraction into an organic phase (toluene). Upon analysis, a single peak at 5.6 min, which consistently represented $\geq 98\%$ of the total chromatograph peak integration, was observed. This peak was identical to fullerenes dissolved in toluene that had not been exposed to water (one peak at 5.6 min (at 336 nm, 4.6×250 mm Cosmosil PYE column, 1 mL/min toluene) with a characteristic C_{60} absorption spectra including peaks at 336, 407,

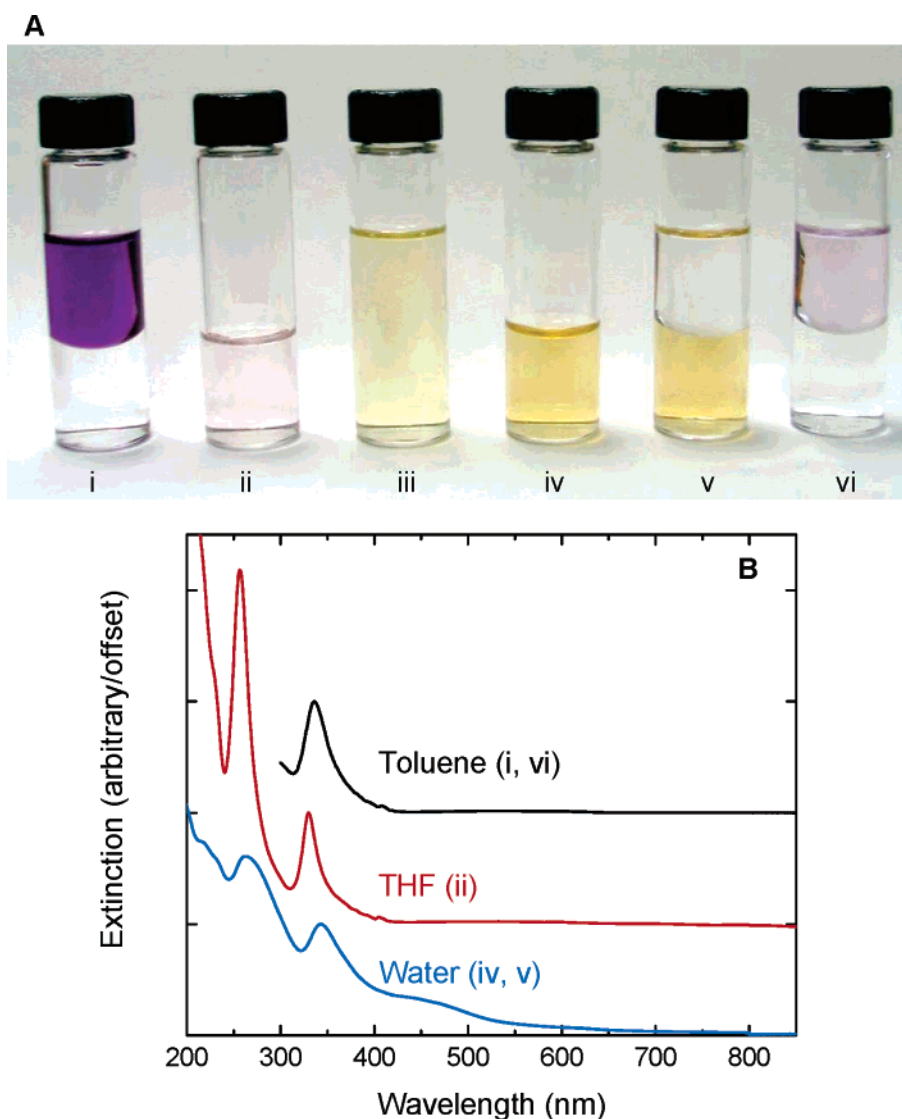


FIGURE 1. Visual and spectral analysis of C_{60} dissolved or in colloidal form in various solvents. (A) C_{60} dissolved in toluene (top) does not partition appreciably into water (bottom) (i). C_{60} dissolved in THF (ii). Water is added to the C_{60} /THF solution, resulting in a yellow suspension of C_{60} nanoparticles (nano- C_{60}) (iii). THF can be evaporated, resulting in a water suspension of nano- C_{60} in only water (iv). The nano- C_{60} in water (bottom) only very slowly dissolves into organic solvents such as toluene (top) (v); the addition of oxidant drives the fullerenes back into the organic phase (vi). (B) UV/Vis analysis of C_{60} dissolved in toluene (top), in THF (middle), and in colloidal form suspended in water (bottom).

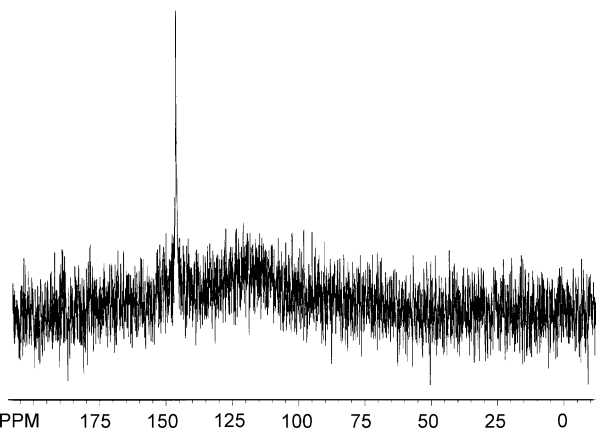


FIGURE 2. ^{13}C NMR spectrum of ^{13}C -labeled (25%) nano- C_{60} suspended in D_2O . A single peak is observed at 146 ppm.

540, and 595 nm) (30, 37, 38) Additionally, ^{13}C NMR analysis indicates that C_{60} remains, within our ability to detect, underivatized in these aggregates. ^{13}C NMR is quite sensitive to derivatization, and fullerenes that have been chemically altered show multiple peaks, often broadened depending on the specificity of the chemistry (38–42). In the case of nano- C_{60} in aqueous suspensions, the spectrum shows only one peak at 146 ppm (Figure 2), which is slightly shifted from solid-state NMR of crystalline, bulk C_{60} which reports a single peak at 143 ppm (40). Thermogravimetric analysis (TGA) and mass spectroscopy of solids recovered from the suspensions are consistent with these findings. The only non-fullerene species present are <10% (w/w) organic molecules, found as THF (data not shown). This is not surprising as the starting powders of polycrystalline C_{60} are known to contain organic molecules intercalated into its lattice, sometimes in relatively high amounts (~10%) (43).

The surface chemistry of these aggregate species is of great interest as it is this interface where the hydrophobic fullerenes are in some way rendered hydrophilic. We confirmed that the surfaces of these materials are charged by performing electrophoretic mobility studies. In agreement with prior studies, we find ζ potentials of -36 mV for a typical suspension produced with water at pH 5 mixed at 500 mL/min (17–19). This weakly charged surface makes these systems unstable in the presence of both weak oxidizing agents and salts.

Two possible explanations could account for the surface charge. It may be that, upon contact with water, pristine fullerenes undergo a chemical reaction to create a small population of partially oxidized, and hence more polar, amphiphilic fullerenes that are able to stabilize the hydrophobic, underivatized core. C_{60} is a relatively reactive species; its degradation by light and oxygen has been noted (44, 45). In particular, one inefficient method to form partially hydroxylated fullerenes relies on the introduction of THF/ C_{60} solutions to water at high pH values (>12) (46). Such a reaction may also proceed, albeit at lower yields, when THF/ C_{60} solutions are introduced in neutral water. Alternatively, C_{60} is an excellent electron acceptor. Both Andrievsky et al. (16) and Deguchi et al. (19) suggested that water itself may form a donor–acceptor complex with C_{60} leading to a weakly charged colloid (21). The latter seems a more reasonable explanation based on the information provided by ^{13}C NMR analysis in Figure 2, which observes a slightly shifted, single peak at 146 ppm, indicating I_h symmetry, which is reserved for underivatized C_{60} (47). In addition, this hypothesis is strengthened by the extraction procedure, as the removal of electrons from the surface via a mild oxidizing agent is necessary to destabilize nano- C_{60} , allowing for virtually all C_{60} to be extracted into an organic phase (toluene). The role

TABLE 1. Bacterial Response to Nano- C_{60} under both Aerobic and Anaerobic Conditions in Different Media^a

media + fullerene	<i>Escherichia coli</i>		<i>Bacillus subtilis</i>	
	aerobic	anaerobic	aerobic	anaerobic
MD (negative control)	+	+	+	+
MD + 0.04 mg/L nano- C_{60}	+	+	+	+
MD + 0.4 mg/L nano- C_{60}	–	–	–	–
MD + 4 mg/L nano- C_{60}	–	–	–	–
MD + 5 mg/L $\text{C}_{60}(\text{OH})_{24}$	+	+	+	+
LB(negative control)	+	+	+	+
LB + 2.5 mg/L nano- C_{60}	+	+	+	+

^a MD is minimal Davis media defined in the Materials and Methods. LB is Luria broth. Results shown as (+) indicate growth and as (–) indicate no growth as measured by optical density at 600 nm. All results reported were the same with or without light present.

of associated organic molecules, such as THF, in the stabilization process would seem to be minor, being that similar suspensions can be made by simply rapidly stirring solid C_{60} in water over time with no intermediate solvent involved (48).

Another outstanding question about these aggregates has been their structure in solution. Past work has shown that both optical and microscopic analyses of the yellow suspensions indicate the presence of dense aggregates of C_{60} (18–20), their form has been challenging to elucidate in solution. Previous reports have first evaporated solutions to form dried films and then used transmission electron microscopy to visualize particles (19, 20). Whether the same particles are present, in the same form and size, in the original solutions was not tested.

Here, we use cryogenic techniques to form flash-frozen suspensions of nano- C_{60} for imaging. This method is widely used in biological systems and has been shown quite often that with rapid freezing the tertiary and quaternary structure of biological molecules remain unaffected (49–51). Transmission electron micrographs of these suspensions are compared to data from dried films (Figure 3A), revealing identical size and morphology, as a large fraction of faceted particles are apparent in the cryogenic suspensions. Under these formation conditions (pH 5 water added at 500 mL/min), nano- C_{60} exhibits a range of sizes, $100 \text{ nm} \pm 10 \text{ nm}$ for these conditions, as well as shapes. Smaller aggregates are typically circular in cross section, intermediate and large particles are mostly rectangular, and the very largest particles often appear to be triangular (Figure 3B). These findings provide direct evidence of particle integrity in suspension, verifying previous studies which have relied on traditional TEM analysis of dried aggregates (18, 20). The particle characteristics suggest that the aggregates are crystalline, and we confirmed this using electron diffraction. SAED on both single particles, as well as particle fields, yields strong diffraction patterns (Figure 3A, inset). Indexing results on a single particle diffraction pattern, taken along the (0001) axis, are most consistent with a simple hexagonal unit cell ($a = 9.4 \text{ \AA}$ and $c/a = 1.09$).

We have found that nano- C_{60} can form over a wide range of mixing conditions and pH and is quite stable at ionic strengths, at or below 0.05 I, for months. Andrievsky et al. (21) suggested that pH was an important parameter for these colloids because of the stability of the surface charge. We found that for pH values between 3.75 and 10.25, nano- C_{60} is formed and that, as the pH of the water is varied, a change in the average particle size is observed. Higher pH values result in smaller nano- C_{60} populations and lower pH values give rise to larger particle populations (Figure 4A,C). In addition, as the pH is increased and the average particle size is smaller, a blue shift in the UV/Vis spectrum is observed in the 330–350 nm range (Figure 4B).

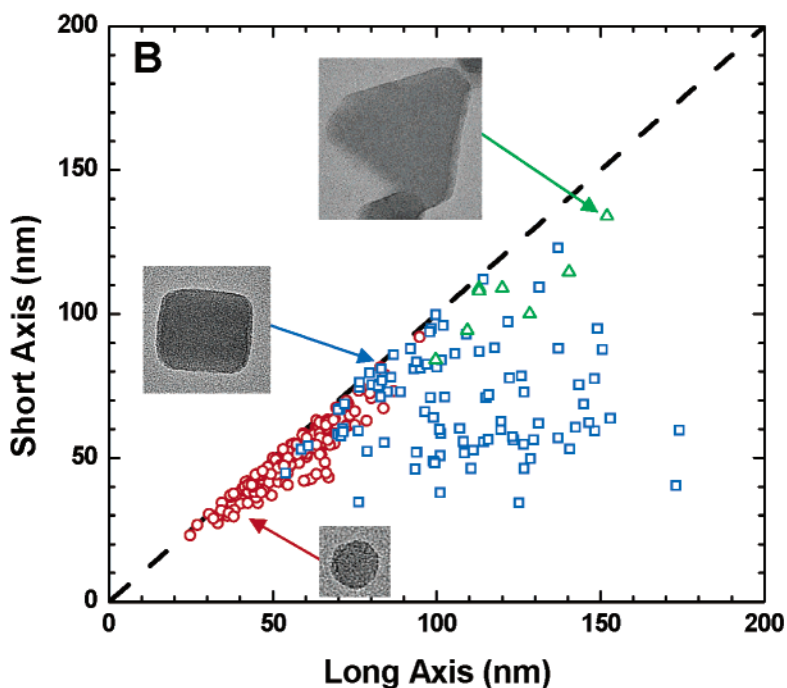
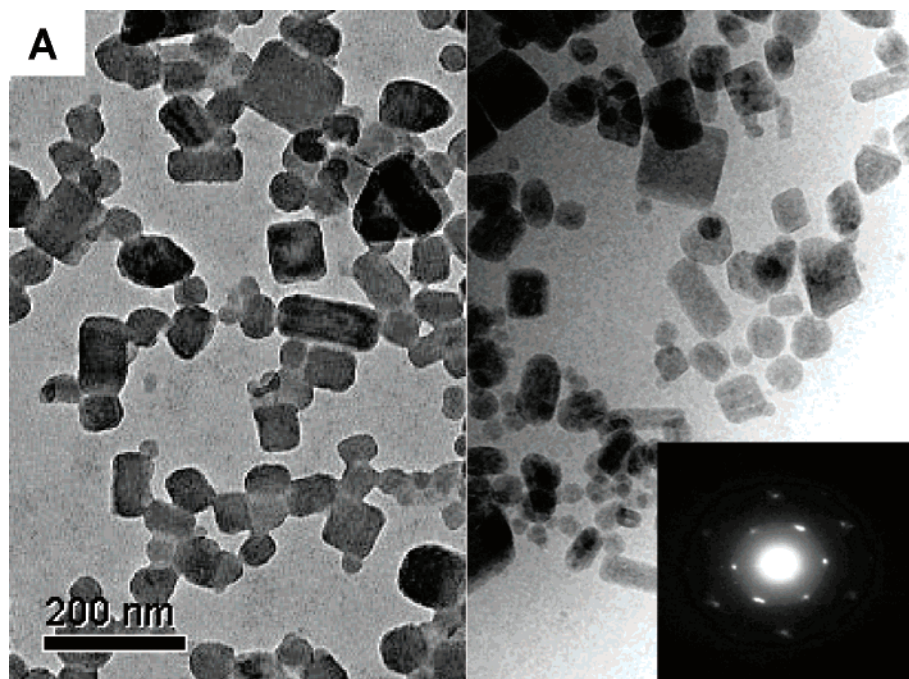


FIGURE 3. Electron microscopy and diffraction analysis of nano- C_{60} . (A) Transmission electron micrographs of dried (left) and flash-frozen (right) samples of nano- C_{60} reveal identical morphology including a large fraction of faceted particles. Electron diffraction on individual particles (inset). (B) Particle size and shape distribution. Small aggregates are typically circular in cross section, intermediate and large ones tending to be rectangular, and with a small fraction of triangular larger particles.

Similarly, we also observed that formation of these particles can be affected by mixing processes involved (i.e., the rate of addition of the water during synthesis) (Figure 5). By increasing or decreasing the rate of water addition, the average particle size varies as observed via DLS and TEM analysis (Figure 5A,C). As the rate of water addition is slowed, average particle size clearly increases. Again, as the average particle size decreases, a blue shift is observed in the 330–350 range (Figure 5B). We note the similar findings by Alargova et al. (18) based on the initial concentration of the C_{60} in the organic phase before the colloids are formed.

Over a range (0.7–0.001 I) of ionic strengths, which includes approximately seawater (0.7) and groundwater (0.01) values, the stability of a typical suspension of nano- C_{60} was evaluated. Results indicate that ionic strengths at 0.05 I and above increase the observed particle size; ionic strengths of 0.1 and 0.7 are high enough to precipitate the particles out of solution after 72 and 48 h, respectively. However, at ionic strengths of 0.001, 0.01, and 0.05 a considerable fraction of the particles remain stable at concentrations up to 100 ppm for at least 15 weeks (Figure 6). It should be noted that these aggregation and stability experiments are not assumed to be

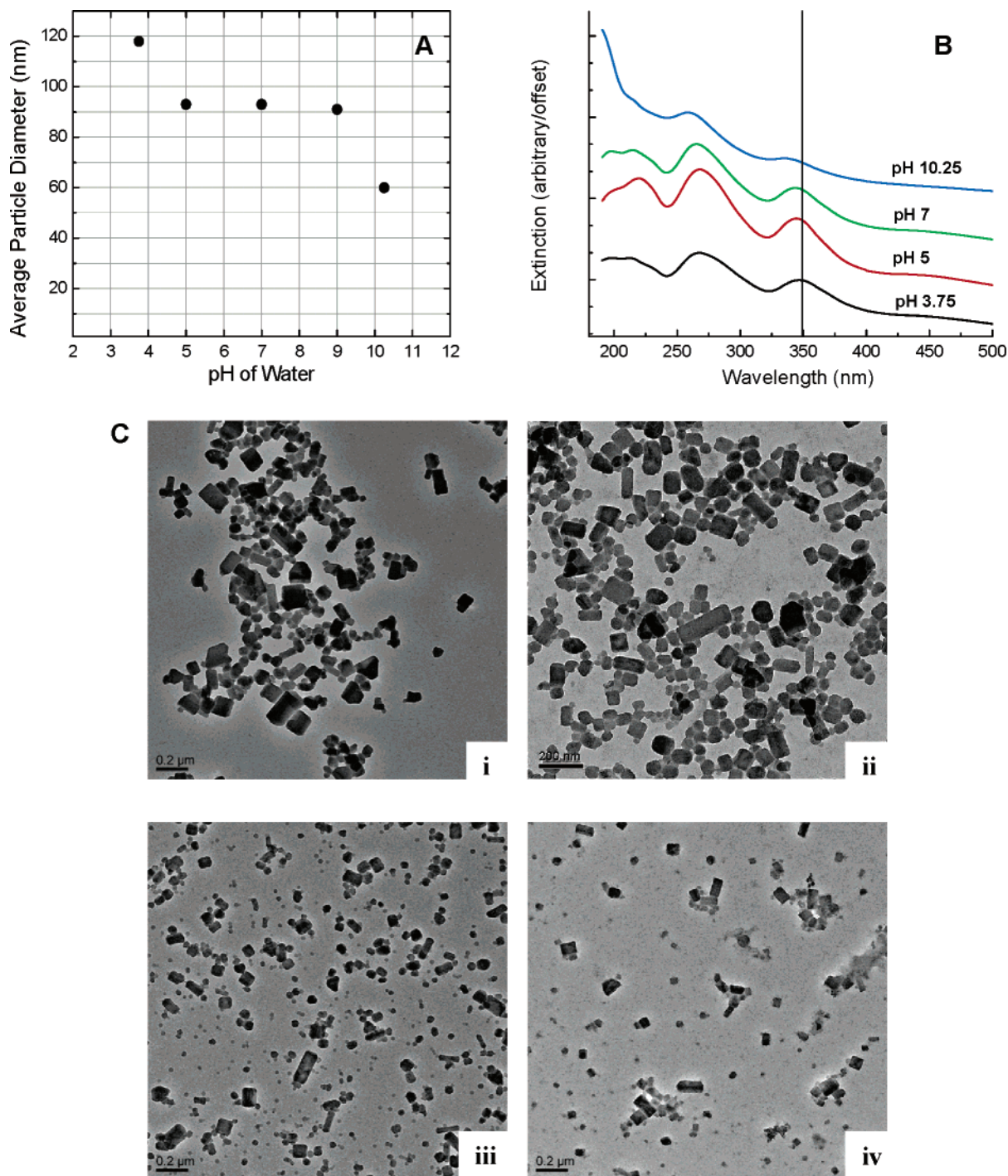


FIGURE 4. Effect of pH during the synthesis of nano-C₆₀. (A) DLS average particle size (nm) value as a function of the pH of the water added during formation. (B) UV/Vis absorption spectra of suspensions made with pH 10.25, 7, 5, and 3.75. Note the blue shift in the 330–350 nm region as the pH is increased. All spectra are offset with arbitrary adsorption units assigned. (C) Dried TEM images of these nano-C₆₀ suspensions: (i) Prepared at pH 3.75. (ii) Prepared at pH 5. (iii) Prepared at pH 7. (iv) Prepared at pH 10.25.

representative of a C₆₀ release into a natural system, as they are more fundamental in approach. The matrix of variables tested does however provide a range of conditions within those found in nature.

With this information about the physical structure, chemical properties, and stability in hand, we examined the biological effects of nano-C₆₀ using two common bacteria. Prokaryotic interactions with nano-C₆₀ were evaluated using the bacteria cultures: Gram-negative *E. coli* and Gram-positive *B. subtilis*, both common, well-studied, soil species, with basic differences in cell wall composition. Initial experiments were designed to observe a bacterial response,

indicated by growth or no growth, to nano-C₆₀ in two different types of media, one complex and one simple, under both anaerobic and aerobic conditions (Table 1). Results show that in the presence of nano-C₆₀ above 0.4 mg/L no growth for either culture is observed (under either anaerobic or aerobic conditions) using a MD media (defined previously). However, when a complex media such as LB was used, growth was seen at nano-C₆₀ concentrations at and below 2.5 mg/L. Subsequent aerobic experiments studied carbon dioxide production during aerobic respiration by these same cultures after exposure to nano-C₆₀ during exponential growth in MD media (Figure 7). Similar studies monitoring CO₂ production

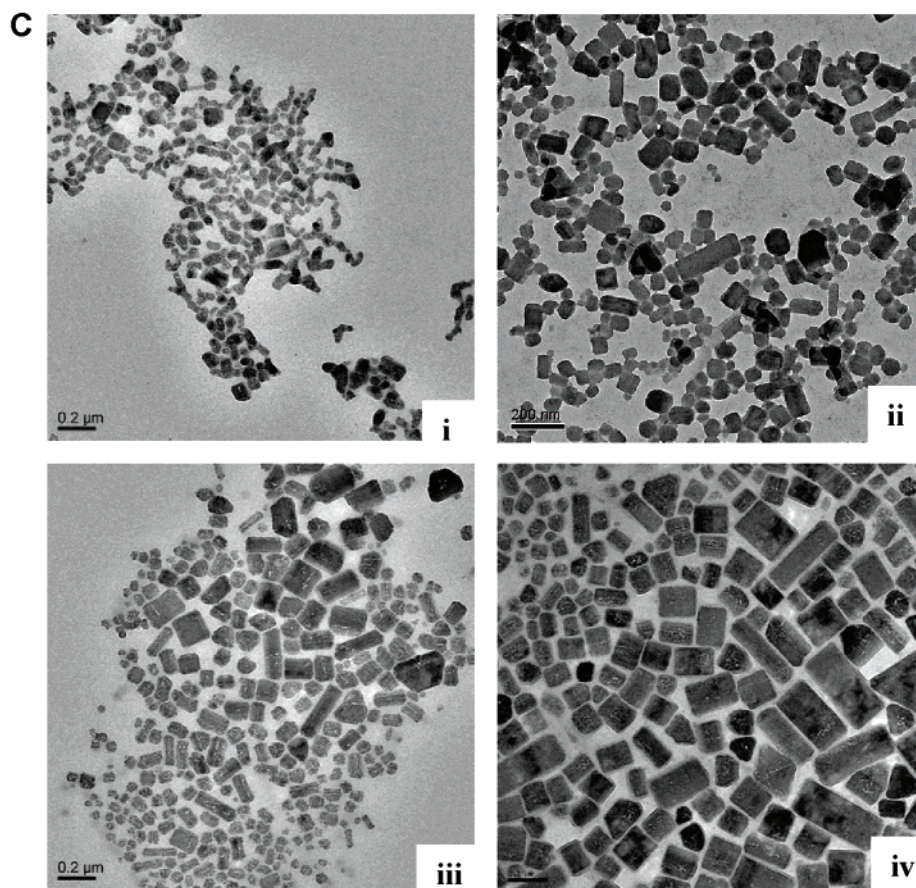
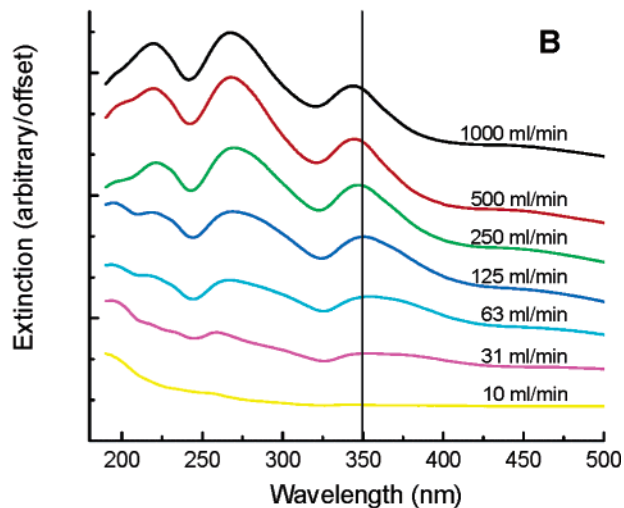
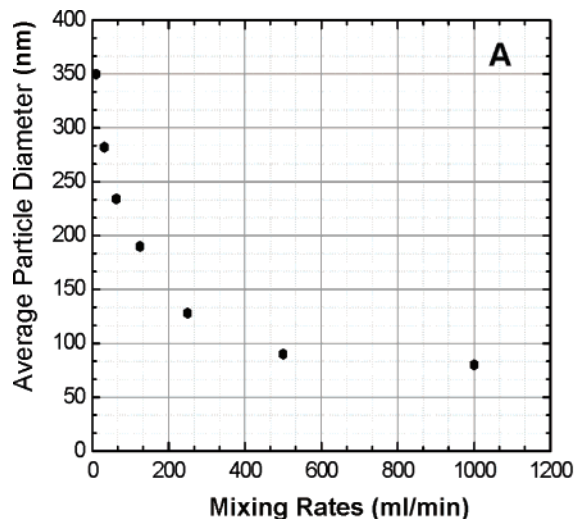


FIGURE 5. Effect of the rate of water addition during the synthesis of nano- C_{60} . (A) DLS average particle size (nm) value as a function of the rate of water addition during the formation process. (B) UV/Vis absorption spectrums of suspensions. Note the blue shift in the 330–350 nm region as the rate is increased. All spectra are offset with arbitrary adsorption units assigned. (C) Representative dried TEM images of these nano- C_{60} suspensions: (i) Prepared at 1000 mL/min. (ii) Prepared at 500 mL/min. (iii) Prepared at 250 mL/min. (iv) Prepared at 63 mL/min.

have been used as a tool in assessing microbial inhibition by others (34, 52). Results presented in Figure 7 are a representative response observed during a 10-chamber experiment (in duplicate, 4 variables and 1 negative control simultaneously monitored with average values presented). All experiments were repeated at least three times verifying the trends observed. These results are consistent with the initial findings that with the addition of nano- C_{60} , at moderately low concentrations (4 mg/L), an adverse effect is observed, indicated by the differential rates of CO_2 production over

time as compared to $C_{60}(OH)_{22-24}$ and a negative control consisting of no fullerenes.

Discussion

As shown here and elsewhere, C_{60} upon contact with water can form negatively charged colloids, nanoscale in dimension, which are stable over time. Specific findings here present strong evidence that in solution, nano- C_{60} is in fact crystalline in order with a simple hexagonal unit cell, and not low density amorphous aggregates, which are not large enough to settle

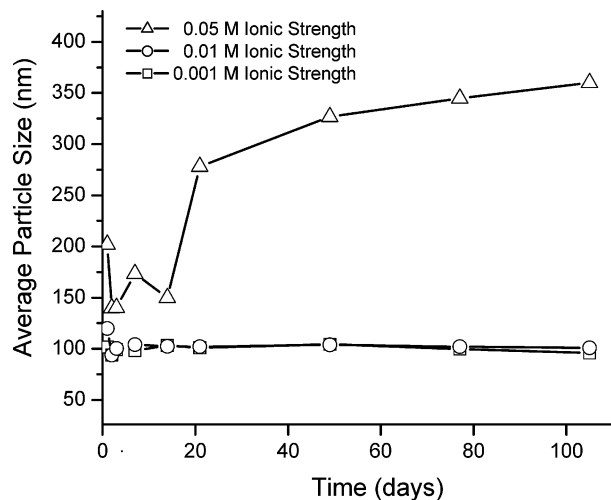


FIGURE 6. Ionic strength and the stability of nano- C_{60} after synthesis. DLS average particle size value was used to assess the stability of the particles in solutions of varying ionic strengths (0.05 I (Δ), 0.01 I (\circ), 0.001 I (\square)) over the course of 15 weeks. Ionic strengths of 0.7 and 0.1 are not shown as nano- C_{60} precipitated out over the course of 48 and 72 h, respectively.

under gravitational force alone. Furthermore, all compositional analyses employed, particularly ^{13}C NMR solution analysis, indicate, that within the margin of error, these colloids are comprised of underivatized C_{60} . These compositional findings, taken with the fact that an oxidizing agent efficiently destabilizes the colloid allowing for toluene extraction of underivatized C_{60} , support the hypothesis suggested by others that a donor-acceptor complex with water may be responsible for the surface charge by which the colloids are stable (16, 18, 19).

It was also found that that the formation process is dynamic. Data presented here, along with a recent study by Alargova et al. (18), outline a number of variables, including initial C_{60} concentration, specific solvents involved, formation kinetics, and chemistry of the water that play a role in the formation process. In particular, we have found that there is a distinct correlation between the rate of water addition and aggregate size, as shown in Figure 5. It appears that the formation of these aggregates is, in part, kinetically controlled by the solution chemistry involved (i.e., as the rate of water

added was increased in the formation process, smaller sized particles were consistently produced). Corresponding formation under conditions of a slow water addition reveals larger average particle populations. Additionally, we found that over a range of pH values (3.75–10.25) nano- C_{60} was formed and that the pH of the water did seem to influence the process as the average particle size decreased with an increase in pH.

Investigations of particle stability at relevant ionic strengths revealed that these aggregates will not remain in solutions simulating seawater or even brackish waters with ionic strengths at or above 0.1 I . However, at ionic strengths below this (0.05 I and below) an appreciable percentage (0.05 I) if not all (0.01 and 0.001 I) of aggregates remain stable for 15 weeks. These results are important as potential long-term stability is limited to aqueous systems at or below 0.05 I , which includes most freshwater environments such as typical groundwaters and surface waters. This study did not investigate other coagulating factors, such as protein, humic acids, or sorption onto or within solid matrixes such as organic matter and soil fractions, which may influence stability.

Bacterial systems employed in this study demonstrate a response to nano- C_{60} at low concentrations. At relatively low concentrations (≥ 0.4 mg/L), nano- C_{60} in a minimal media does induce a response by common Gram-positive and Gram-negative cultures, indicated by the lack of growth in a variety of basic conditions, including aerobic or anaerobic conditions and with or without the presence of light (Table 1). However, complex media (LB) seemed to negate this response by perhaps salting the fullerenes out of solution, as shown here at higher ionic strengths in Figure 6 or through coating the fullerenes with excess protein, which is a large component of this particular media (as yeast extract). Furthermore, these results were corroborated with respiration studies (Figure 7) showing similar response at comparable concentrations, as rates of CO_2 production decrease with the introduction of nano- C_{60} during the exponential growth phase. In addition, for both cultures, when exposed to similar concentrations of a hydroxylated fullerene $C_{60}(OH)_{22-24}$ no significant response in bacterial respiration was observed, confirmed by a negative control lacking fullerenes, suggesting a relation in the surface chemistry of the fullerene molecules to the biological activity. These initial data are the first examination of a microbial response to nano- C_{60} and are consistent with published data by Sayes et al. (9), which

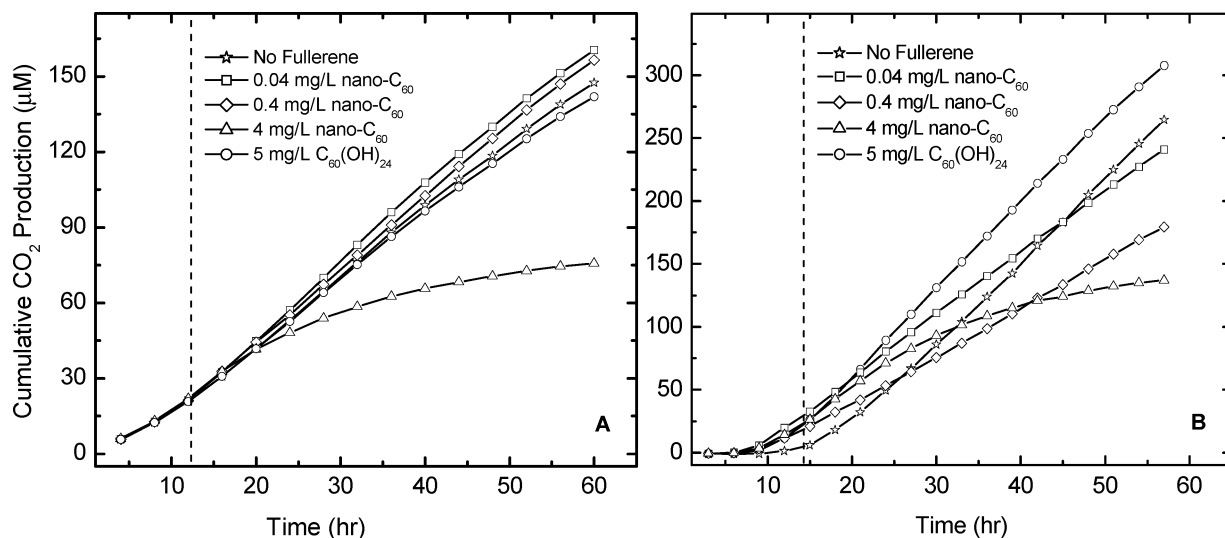


FIGURE 7. Response of Gram-negative *Escherichia coli* (A) and Gram-positive *Bacillus subtilis* (B) to nano- C_{60} as measured by aerobic respiration rates. Nano- C_{60} was administered to the cultures early in the exponential growth phase indicated by the dotted line. Respiration is shown as average (run in duplicate) production of CO_2 expressed as total accumulation, rates correspond to the slope.

demonstrated nano-C₆₀ toxicity to human dermal fibroblasts (HDF) diminishing with an increase in derivatization (as hydroxylation).

In aqueous systems, nano-C₆₀ behaves neither as an individual molecule nor as a bulk solid. Moreover, chemical properties of the aggregate, such as partition coefficients, are distinct from individual C₆₀ molecules. On the basis of the predicted widespread use of C₆₀, this becomes a particularly striking observation that deviates from that which is expected for similar materials such as hydrophobic polyaromatic hydrocarbons (PAHs). In this case, predictive molecular properties such as partition coefficients (*K_{ow}*) and solubility become inappropriate, with colloidal properties such as size and surface chemistry becoming useful in predicting behavior of these aggregates. Moreover, recent reports by Lecoanet and Wiesner (53) studying the mobility of suspended nanomaterials in porous media show that similar C₆₀ aggregates are capable of migrating through a well-defined porous medium analogous to a sandy ground-water aquifer.

This work clearly illustrates the limitations of the current guidelines for the handling and disposal of C₆₀, which are based entirely on the properties of bulk carbon black. Most engineered nanomaterials, including C₆₀, are handled and disposed according to guidelines established for their bulk counterparts; these guidelines may need to be revisited. Proactive characterization of the environmental chemistry and associated ecological risk of engineered nanomaterials, before their use is widespread, ensures an environmentally sustainable, and socially beneficial nanotechnology industry.

Acknowledgments

This research was funded through the Nanoscale Science and Engineering Initiative of the National Science Foundation (EEC-0118007). Additionally, we acknowledge funding for NMR analysis through NSF CHE-9708978.

Literature Cited

- (1) Kelty, S. P.; Chen, C. C.; Lieber, C. M. Superconductivity at 30-K in cesium-doped C₆₀. *Nature* **1991**, *352*, 223–225.
- (2) Kroto, H. W.; Heath, J. R.; O'Brien, S. C.; Curl, R. F.; Smalley, R. E. C₆₀: Buckminsterfullerene. *Nature* **1985**, *318*, 162.
- (3) Tsao, N.; Kanakamma, P. P.; Luh, T. Y.; Chou, C. K.; Lei, H. Y. Inhibition of *Escherichia coli*-induced meningitis by carboxyfullerene. *Antimicrob. Agents Chemother.* **1999**, *43*, 2273–2277.
- (4) Haddon, R. C.; Hebard, A. F.; Rosseinsky, M. J.; Murphy, D. W.; Duclos, S. J.; Lyons, K. B.; Miller, B.; Rosamilia, J. M.; Fleming, R. M.; Kortan, A. R.; Glarum, S. H.; Makhija, A. V.; Muller, A. J.; Eick, R. H.; Zahurak, S. M.; Tycko, R.; Dabbagh, G.; Thiel, F. A. Conducting films of C₆₀ and C₇₀ by alkali-metal doping. *Nature* **1991**, *350*, 320–322.
- (5) Ruoff, R. S.; Ruoff, A. L. Is C₆₀ stiffer than diamond. *Nature* **1991**, *350*, 663–664.
- (6) Innocenzi, P.; Brusatin, G. Fullerene-based organic–inorganic nanocomposites and their applications. *Chem. Mater.* **2001**, *13*, 3126–3139.
- (7) Ungurenasu, C.; Airinei, A. Highly stable C₆₀/poly(vinylpyrrolidone) charge-transfer complexes afford new predictions for biological applications of underivatized fullerenes. *J. Med. Chem.* **2000**, *43*, 3186–3199.
- (8) Tremblay, J. Mitsubishi aims at a breakthrough. *Chem. Eng. News* **2002**, *80*, 16–17.
- (9) Sayes, C. M.; Fortner, J. D.; Guo, W.; Lyon, D.; Boyd, A. M.; Ausman, K. D.; Tao, Y. J.; Sitharaman, B.; Wilson, L. J.; Hughes, J. B.; West, J. L.; Colvin, V. L. The differential cytotoxicity of water-soluble fullerenes. *Nanolett.* **2004**, *4*, 1881–1887.
- (10) Oberdörster, E. Manufactured nanomaterials (fullerenes, C₆₀) induce oxidative stress in the brain of juvenile largemouth bass. *Environ. Health Perspect.* **2004**, *112*, 1058–1062.
- (11) Utsunomiya, S.; Jensen, K. A.; Keeler, G. J.; Ewing, R. C. Uraninite and fullerene in atmospheric particles. *Environ. Sci. Technol.* **2002**, *36*, 4943–4947.
- (12) Ruoff, R. S.; Tse, D. S.; Malhotra, R.; Lorents, D. C. Solubility of C₆₀ in a variety of solvents. *J. Phys. Chem.* **1993**, *97*, 3379–3383.
- (13) Heymann, D. solubility of C₆₀ in alcohols and alkanes. *Carbon* **1996**, *34*, 627–631.
- (14) Heymann, D. Solubility of C₆₀ and C₇₀ in seven normal alcohols and their deduced solubility in water. *Fullerene Sci. Technol.* **1996**, *4*, 509–515.
- (15) Scrivens, W. A.; Tour, J. M. Synthesis of ¹⁴C-labeled C₆₀, its suspension in water, and its uptake by human keratinocytes. *J. Am. Chem. Soc.* **1994**, *116*, 4517–4518.
- (16) Andrievsky, G. V.; Kosevich, M. V.; Vovk, O. M.; Shelkovsky, V. S.; Vashchenko, L. A. On the production of an aqueous colloidal solution of fullerenes. *J. Chem. Soc. Commun.* **1995**, 1281–1282.
- (17) Mchedlov-Petrosyan, N. O.; Klochkov, V. K.; Andrievsky, G. V. Colloidal dispersions of fullerene C₆₀ in water: Some properties and regularities of coagulation by electrolytes. *J. Chem. Soc. Faraday Trans.* **1997**, *93*, 4343–4346.
- (18) Alargova, R. G.; Deguchi, S.; Tsujii, K. Stable colloidal dispersions of fullerenes in polar organic solvents. *J. Am. Chem. Soc.* **2001**, *123*, 10460–10467.
- (19) Deguchi, S.; Alargova, R. G.; Tsujii, K. Stable dispersions of fullerenes, C₆₀ and C₇₀, in water. Preparation and characterization. *Langmuir* **2001**, *17*, 6013–6017.
- (20) Andrievsky, G. V.; Klochkov, V. K.; Karyakina, E. L.; Mchedlov-Petrosyan, N. O. Studies of aqueous colloidal solutions of fullerene C-60 by electron microscopy. *Chem. Phys. Lett.* **1999**, *300*, 392–396.
- (21) Andrievsky, G. V.; Klochkov, V. K.; Bordyuh, A. B.; Dovbeshko, G. I. Comparative analysis of two aqueous-colloidal solutions of C₆₀ fullerene with help of FTIR reflectance and UV–Vis spectroscopy. *Chem. Phys. Lett.* **2002**, *364*, 8–17.
- (22) Li, T. B.; Huang, K. X.; Li, X. H.; Jiang, H. Y.; Li, J.; Yan, X. Z.; Zhao, S. K. Studies on the rapid preparation of fullerenols and its formation mechanism. *Chem. Res. Chin. Univ.* **1998**, *19*, 858–860 (in Chinese).
- (23) Chiang, L. Y.; Upasani, R. B.; Swirezewski, J. W.; Soled, S. Evidence of hemiketals incorporated in the structure of fullerols derived from aqueous acid chemistry. *J. Am. Chem. Soc.* **1993**, *115*, 5453–5457.
- (24) Schneider, N. S.; Darwish, A. D.; Kroto, H. W.; Taylor, R.; Walton, D. R. M. Formation of fullerols via hydroboration of fullerene-C₆₀. *J. Chem. Soc., Chem. Commun.* **1994**, *4*, 463–464.
- (25) Arrais, A.; Diana, E. Highly water soluble C₆₀ derivatives: A new synthesis. *Fullerenes Nanotubes Carbon Nanostruct.* **2003**, *11*, 35–46.
- (26) Cusan, C.; Da Ros, T.; Spalluto, G.; Foley, S.; Janto, J. M.; Seta, P.; Larroque, C.; Tomasini, M. C.; Antonelli, T.; Ferraro, L.; Prato, M. A new multi-charged C₆₀ derivative: Synthesis and biological properties. *Eur. J. Org. Chem.* **2002**, 2928–2934.
- (27) Da Ros, T.; Prato, M. Easy access to water-soluble fullerene derivatives via 1,3-dipolar cycloadditions of azomethine ylides to C. *J. Org. Chem.* **1996**, *61*, 9070–9072.
- (28) Chung, N.; Alexander, M. Effect on Sequestration and bioavailability of two polycyclic aromatic hydrocarbons. *Environ. Sci. Technol.* **1999**, *33*, 3605–3608.
- (29) Djordjevic, A.; Vojinovic-Milofadov, M.; Petranovic, N.; Devecerski, A.; Bogdanovic, G.; Adamov, J. Synthesis and characterization of water-soluble biologically active C₆₀(OH)₂₄. *Arch. Oncol.* **1997**, *5*, 139–142.
- (30) Wu, Y. Q.; Sun, Y. L.; Gu, Z. N.; Wang, Q. W.; Zhou, X. H.; Xiong, Y.; Jin, Z. X. Analysis of C₆₀ and C₇₀ fullerenes by high-performance liquid-chromatography. *J. Chromatogr.* **1993**, *648*, 491–496.
- (31) Hoffmann, T.; Frankenberg, N.; Marino, M.; Jahn, D. Ammonification in *Bacillus subtilis* utilizing dissimilatory nitrite reductase is dependent on resDE. *J. Bacteriol.* **1998**, *180*, 186–189.
- (32) Atlas, R. M. *Handbook of Microbiological Media*; CRC Press: Boca Raton, FL, 1993.
- (33) Marino, M.; Ramos, H. C.; Hoffmann, T.; Glaser, P.; Jahn, D. Modulation of anaerobic energy metabolism of *Bacillus subtilis* by arfM (ywiD). *J. Bacteriol.* **2001**, *183*, 6815–6821.
- (34) Fortner, J. D.; Zhang, C. L.; Spain, J. C.; Hughes, J. B. Soil column evaluation of factors controlling biodegradation of DNT in the vadose zone. *Environ. Sci. Technol.* **2003**, *37*, 3382–3391.
- (35) Bensasson, R. V.; Bienvenue, E.; Dellinger, M.; Leach, S.; Seta, P. C₆₀ in model biological-systems. A visible-UV absorption study of solvent-dependent parameters and solute aggregation. *J. Phys. Chem.* **1994**, *98*, 3492–3500.
- (36) Hungerbühler, H.; Guldi, D. M.; Asmus, K.-D. Incorporation of C₆₀ into artificial membranes. *J. Am. Chem. Soc.* **1993**, *115*, 3386–3387.

- (37) Cox, D. M.; Behal, S.; Disko, M.; Gorun, S. M.; Greaney, M.; Hsu, C. S.; Kollin, E. B.; Millar, J.; Robbins, J.; Robbins, W.; Sherwood, R. D.; Tindall, P. Characterization of C₆₀ and C₇₀ clusters. *J. Am. Chem. Soc.* **1991**, *113*, 2940–2944.
- (38) Gu, Z. N.; Qian, J. X.; Zhou, X. H.; Wu, Y. Q.; Zhu, X.; Feng, S. Q.; Gan, Z. Z. Buckminsterfullerene C₆₀—synthesis, spectroscopic characterization, and structure analysis. *J. Phys. Chem.* **1991**, *95*, 9615–9618.
- (39) Balch, A. L.; Costa, D. A.; Noll, B. C.; Olmstead, M. M. Oxidation of Buckminsterfullerene with *m*-chloroperoxybenzoic acid—characterization of a C–S isomer of the diepoxide C₆₀O₂. *J. Am. Chem. Soc.* **1995**, *117*, 8926–8932.
- (40) Yannoni, C. S.; Johnson, R. D.; Meijer, G.; Bethune, D. S.; Salem, J. R. C-13 NMR study of the C₆₀ cluster in the solid-state—molecular-motion and carbon chemical-shift anisotropy. *J. Phys. Chem.* **1991**, *95*, 9–10.
- (41) Johnson, R. D.; Yannoni, C. S.; Dorn, H. C.; Salem, J. R.; Bethune, D. S. C-60 rotation in the solid-state—dynamics of a faceted spherical top. *Science* **1992**, *255*, 1235–1238.
- (42) Doome, R. J.; Fonseca, A.; Nagy, J. B.; Grell, A. S.; Masin, F.; Messari, I. NMR answer to the anomalous solubility behaviour of fullerenes. *Mol. Mater.* **2000**, *13*, 201–208.
- (43) Skokan, E. V.; Privalov, V. I.; Arkhangel'skii, I. V.; Davydov, V. Y.; Tamm, N. B. Solvent molecules in crystalline C₆₀. *J. Phys. Chem. B* **1999**, *103*, 2050–2053.
- (44) Diederich, F.; Thilgen, C. Covalent fullerene chemistry. *Science* **1996**, *271*, 317–323.
- (45) Taylor, R.; Parsons, J. P.; Avent, A. G.; Rannard, S. P.; Dennis, T. J.; Hare, J. P.; Kroto, H. W.; Walton, D. R. M. Degradation of C₆₀ by light. *Nature* **1991**, *351*, 277–277.
- (46) Li, J.; Takeuchi, A.; Ozawa, M.; Li, X.; Saigo, K.; Kitazawa, K. C₆₀ fullerol formation catalysed by quaternary ammonium hydroxide. *J. Am. Chem. Commun.* **1993**, 1784–1786.
- (47) Kratschmer, W.; Lamb, L. D.; Fostiropoulos, K.; Huffman, D. R. Solid C-60—a new form of carbon. *Nature* **1990**, *347*, 354–358.
- (48) Cheng, X. K.; Kan, A. T.; Tomson, M. B. Naphthalene adsorption and desorption from aqueous C₆₀ fullerene. *J. Chem. Eng. Data* **2004**, *49*, 675–683.
- (49) Adrian, M.; Dubochet, J.; Lepault, J.; McDowell, A. W. Cryo-electron microscopy of viruses. *Nature* **1984**, *308*, 32–36.
- (50) Conway, J. F.; Cheng, N.; Zlotnick, A.; Wingfield, P. T.; Stahl, S. J.; Steven, A. C. Visualization of a 4-helix bundle in the hepatitis B virus capsid by cryo-electron microscopy. *Nature* **1997**, *386*, 91–94.
- (51) Prasad, B. V.; Burns, J. W.; Marietta, E.; Estes, M. K.; Chiu, W. Localization of VP4 neutralization sites in rotavirus by three-dimensional cryo-electron microscopy. *Nature* **1990**, *343*, 476–479.
- (52) Georgiou, D.; Melidis, P.; Aivasidis, A. Use of a microbial sensor: Inhibition effect of azo-reactive dyes on activated sludge. *Bioprocess Biosyst. Eng.* **2002**, *25*, 79–83.
- (53) Lecoanet, H. F.; Wiesner, M. R. Velocity effects on fullerene and oxide nanoparticle deposition in porous media. *Environ. Sci. Technol.* **2004**, *38*, 4377–4382.

Received for review December 1, 2004. Revised manuscript received March 9, 2005. Accepted March 18, 2005.

ES048099N